

Bootstrap for lattice Yang-Mills theoryVladimir Kazakov^{1,2,*} and Zechuan Zheng^{1,†}¹*Laboratoire de physique de l'École normale supérieure, ENS, Université PSL, CNRS, Sorbonne Université, Université Paris Cité, 24 rue Lhomond, F-75005 Paris, France*²*Interdisciplinary Scientific Center Poncelet, CNRS UMI 2615, 119002 Moscow, Russia*

(Received 8 May 2022; accepted 30 January 2023; published 9 March 2023)

We study the $SU(\infty)$ lattice Yang-Mills theory at the dimensions $D = 2, 3, 4$ via the numerical bootstrap method. It combines the loop equations, with a cutoff L_{\max} on the maximal length of loops, and positivity conditions on certain matrices of Wilson loop averages. Our algorithm is inspired by the pioneering paper of P. D. Anderson and M. Kruczenski [Nucl. Phys. **B921**, 702 (2017)] but it is significantly more efficient, as it takes into account the symmetries of the lattice theory and uses the relaxation procedure in line with our previous work on matrix bootstrap. We thus obtain rigorous upper and lower bounds on the plaquette average at various couplings and dimensions. For $D = 4$, $L_{\max} = 16$ the lower bound data appear to be close to the Monte Carlo data in the strong coupling phase and the upper bound data in the weak coupling phase reproduce well the 3-loop perturbation theory. Our results suggest that this bootstrap approach can provide a tangible alternative to the, so far uncontested, Monte Carlo approach.

DOI: [10.1103/PhysRevD.107.L051501](https://doi.org/10.1103/PhysRevD.107.L051501)**I. INTRODUCTION**

The $SU(N_c)$ Yang-Mills (YM) lattice gauge theory (LGT) is a fundamental ingredient of modern particle physics. Its most illustrious applications are the Standard Model and, in particular, the quantum chromodynamics. Nowadays, most of the nonperturbative computations in Yang-Mills theory are done by Monte Carlo (MC) simulations for the lattice formulation of YM theory. Combined with perturbation theory (PT) [1–5] and RG tools, MC methods have had a huge success, especially in the recent couple of decades, due to the development of supercomputers. It allowed us to compute, with a reasonable precision, certain masses of hadrons and the S -matrix elements in QCD, reproducing the experimental data [6,7]. However, the absence of any systematic nonperturbative “analytic” alternative to MC is, practically and intellectually, somewhat uncomfortable. Moreover, the MC method has its inherent limitations; statistical errors, finite lattice size, high numerical cost of inclusion of dynamical quarks, difficulties in treating finite baryon density, and the real-time dynamics.

An interesting alternative for the study of the LGT is provided by Makeenko-Migdal loop equations (LE) [8,9] for Wilson loop averages (WA). An early attempt at numerical study of LE in the large N_c , 't Hooft limit was proposed in [10–13], in the form of minimization of effective action in the loop space. A more recent brave attempt to bootstrap the LEs, combining them with certain positivity conditions [14,15], revived hopes of a more analytic approach. Slightly later, a similar bootstrap method was proposed in [16] for the multimatrix models. In our work [17] we significantly improved the matrix bootstrap by introducing a “relaxation” procedure and applied it to an “analytically unsolvable” large N 2-matrix model, with remarkable efficiency and precision, noticeably exceeding those of MC for the same model [18].

These developments have been considerably inspired by the success of the bootstrap approach to conformal field theories (CFTs) [19,20] and S -matrices in massive QFTs [21–23].

Unlike MC where the result is given up to statistical error bars, the bootstrap methods provides rigorous inequalities giving upper and lower bounds on computed physical quantities. These bounds can only improve when increasing the number of bootstrapped variables and constraints on them.

Here we develop a powerful numerical bootstrap algorithm for solving the LEs [8,9] in the lattice YM theory at $N_c \rightarrow \infty$ and demonstrate it on the computation of plaquette average $u_P = \frac{1}{N_c} \langle \text{tr} U_P \rangle$. Its main ingredients are (i) positivity of correlation matrix of WAs; (ii) our

*kazakov@lpt.ens.fr

†zechuan.zheng.phy@gmail.com

Published by the American Physical Society under the terms of the [Creative Commons Attribution 4.0 International license](https://creativecommons.org/licenses/by/4.0/). Further distribution of this work must maintain attribution to the author(s) and the published article's title, journal citation, and DOI. Funded by SCOAP³.

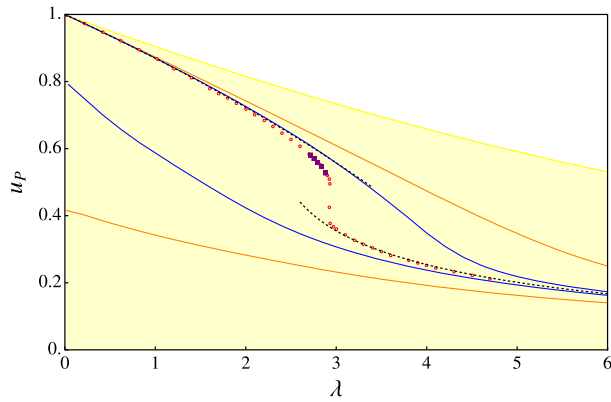


FIG. 1. Our bootstrap results for upper and lower bounds on plaquette average in 4D LGT (1): for $L_{\max} = 8$ (yellow domain) for $L_{\max} = 12$ (orange curves) and $L_{\max} = 16$ (blue curves). Red circles represent the MC data for $SU(10)$ LGT [with five purple squares for $SU(12)$]. Dashed upper and lower lines represent the 3-loop PT (13) and strong coupling expansion (14), respectively.

relaxation procedure of [17]; (iii) positivity of reflection matrices due to lattice symmetries; and (iv) symmetry reduction of the positivity conditions. In the Supplementary Material [24], we worked out a simple example for our general method together with some data points.

Our data (obtained on a single workstation), for the modest length cutoff $L_{\max} = 16$, looked quite encouraging; as seen on Fig. 1, for $D = 4$, our lower (upper) bounds are quite close to the MC data [14,15,25,26] in the strong (weak) coupling phase, at least far enough from the phase transition. The upper bound is remarkably close to the 3-loop PT.

In Fig. 2 we plot the difference of the bootstrap upper bound and the 3-loop PT, $\Delta u_P \equiv u_P^{\text{boot}} - u_P^{\text{PT}}$, as a function of $1/\lambda$. It might capture the nonperturbative effect for the gluon condensate $\langle \text{tr}(F_{\mu\nu} F^{\mu\nu}) \rangle$ —in principal a measurable observable [27–29]. The graph is very smooth and it is positive even slightly beyond the phase transition point $\lambda_c \simeq 2.9$ [30].

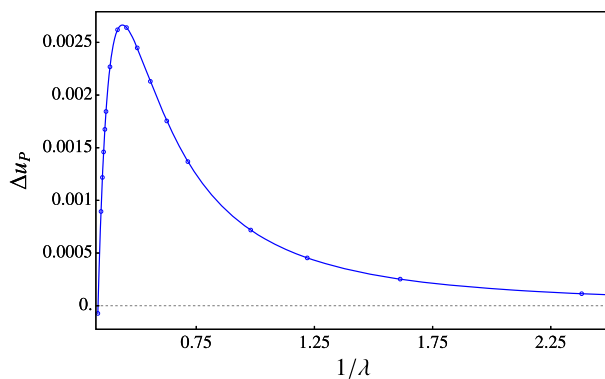


FIG. 2. The plot $\Delta u_P \equiv u_P^{\text{boot}} - u_P^{\text{PT}}$ which might capture the nonperturbative values of the gluon condensate $\langle \text{tr}(F_{\mu\nu} F^{\mu\nu}) \rangle$.

II. YANG-MILLS LOOP EQUATIONS AT LARGE N

We study the LGT with the Wilson action [31]

$$S = -\frac{N_c}{\lambda} \sum_P \text{Re tr} U_P, \quad (1)$$

where U_P is the product of four unitary link variables around the plaquette P and we sum over all plaquettes P , including both orientations. The main quantities of interest in 't Hooft limit $N_c \rightarrow \infty$ are the WAs:

$$W[C] = \left\langle \frac{\text{tr}}{N_c} \prod_{l \in C} U_l \right\rangle. \quad (2)$$

The matrix product goes over the link variables belonging to the lattice loop C . $W[C]$ are subject to LEs, i.e., the Schwinger-Dyson equations expressing measure invariance with respect to group shifts $U_l \rightarrow U_l(1 + i\epsilon)$. Schematically the LE reads,

$$\sum_{\nu \perp \mu} (W[C_{l_\mu} \cdot \overrightarrow{\delta C_{l_\mu}^\nu}] - W[C_{l_\mu} \cdot \overleftarrow{\delta C_{l_\mu}^\nu}]) = \lambda \sum_{\substack{l' \in C \\ l' \sim l}} \epsilon_{ll'} W[C_{ll'}] W[C_{l'l}], \quad (3)$$

where the lhs represents the loop operator acting on the link l_μ by replacing it with the loop around plaquette $\overrightarrow{\delta C_{l_\mu}^\nu}$ or $\overleftarrow{\delta C_{l_\mu}^\nu}$ (depending on the orientation, as shown in the first line of Fig. 3). The lhs sum goes around all $2(D-1)$ $\mu\nu$ -plaquettes orthogonal to the direction μ . The rhs sum goes over all appearances of the same lattice link l in the loop C . The rhs product corresponds to splitting of the contour $C \rightarrow C_{ll'} \cdot C_{l'l}$, as explained in the second and third lines of Fig. 3. Finally, $\epsilon_{ll'} = \pm 1$ for links l and l' with

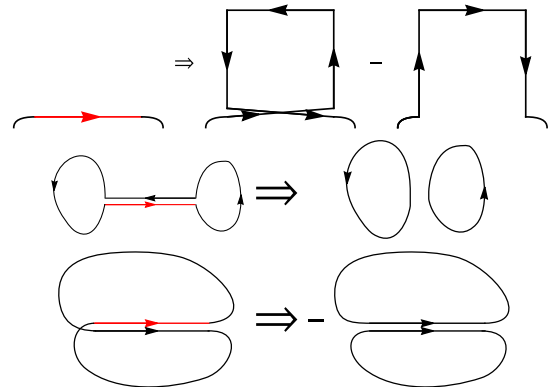


FIG. 3. Schematic representation of LEs. The first line shows the variation of a link of Wilson loop in the LHS of Eq. (3). The second and third lines show the splitting of the contour along the varied line into two sub-contours, for two different orientations of coinciding links in the rhs of Eq. (3).

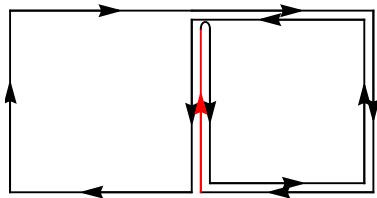


FIG. 4. An example of nonlinear “backtrack” LE.

opposite or collinear orientation, respectively. For more details on LEs, see [14,32,33].

A. Backtrack loop equations

To get the full list of the LEs, we also consider the “backtrack” LEs. They correspond to doing variations on the links at the end of “backtrack” paths originating from the vertices of Wilson loop. These “backtracks” are equivalent to inserting the identity, but their Schwinger-Dyson variation, can give independent LEs. Figure 4 shows an example of “backtrack” LE,

$$\text{Loop} + \text{Loop}_{\text{backtrack}} - \text{Loop}_{\text{backtrack}} - \text{Loop}_{\text{backtrack}} = \lambda u_P \text{Loop}. \quad (4)$$

The LEs close on single trace WAs (2) (due to the large N_c factorization of color traces), which means that they behave as classical quantities on the loop space. At $L_{\max} = 16$, we have about 40,000 LEs in 3D and about 100,000 LEs in 4D, and the backtrack LEs constitute more than 80% of all these LEs. Around three-quarters of them are linearly independent and only a small minority are nonlinear. Finding the solution to these equations is our primary task for any other progress in studying the physical quantities of planar QCD or its $1/N_c$ corrections. The problem is very complicated since it is formulated in extremely complex loop space. We will try to solve it using the bootstrap approach.

III. BOOTSTRAP ALGORITHM

A. Positivity constraints

In general, our positivity conditions come from the positivity of possible inner products on the vector space or a subspace of the operators, i.e.,

$$\langle \mathcal{O} | \mathcal{O} \rangle = \langle \mathcal{O}^\dagger \mathcal{O} \rangle = \alpha^{*\text{T}} \mathcal{M} \alpha \geq 0 \Leftrightarrow \mathcal{M} \geq 0, \quad (5)$$

where $\mathcal{O} = \sum \alpha_i \mathcal{O}_i$ is an operator with arbitrary coefficients α_i , and \mathcal{O}_i are basis vectors of the operators.

One of possible adjoint operators \mathcal{O}^\dagger comes from taking the Hermitian conjugation [14,16,17]. For a Wilson path,

the Hermitian conjugation corresponds to reversing the path. By taking a linear combination of all Wilson paths $0 \rightarrow x$ (between the points 0 and x), with arbitrary coefficients, we can get nontrivial positivity conditions from their inner product. For example, we have only two paths $0 \rightarrow (1, 1)$, at $L_{\max} = 2$

$$\text{Path}_1 = \left[\begin{array}{c} \leftarrow \\ \leftarrow \\ \leftarrow \end{array} \right], \quad \text{Path}_2 = \left[\begin{array}{c} \leftarrow \\ \leftarrow \\ \leftarrow \\ \leftarrow \end{array} \right] \quad (6)$$

and the positivity condition reads,

$$\begin{array}{c} \text{Path}_1^\dagger \\ \text{Path}_2^\dagger \end{array} \begin{array}{cc} \text{Path}_1 & \text{Path}_2 \\ \left(\begin{array}{cc} 1 & u_P \\ u_P & 1 \end{array} \right) & \succeq 0. \end{array} \quad (7)$$

This gives $u_P^2 \leq 1$, obvious from unitarity. We call the positivity matrices arising from the Hermitian conjugation the correlation matrices.

Apart from Hermitian conjugation, we have additional reflection positivity conditions where adjointed operators \mathcal{O}^\dagger come from reflection symmetries [34]. For LGT, there are three types of reflections with respect to different planes; site, link, and diagonal reflections [35,36]. Figure 5 illustrates the corresponding adjoint paths for these reflections. The importance of three new reflection positivity conditions is illustrated in Fig. 6 where we compare $L_{\max} = 12$ bootstrap results with and without reflection positivity.

For computations in this work, we consider the full positivity constraint $0 \rightarrow x$ for any possible x when $L_{\max} \leq 12$. But for $L_{\max} = 16$, we consider only the paths $0 \rightarrow 0$ for various positivity matrices since:

- (1) When constructing correlation matrices, all the positivity conditions on the open Wilson paths $0 \rightarrow x$ are already contained in $0 \rightarrow 0$ correlation matrix for higher lengths (due to backtrackings).
- (2) At $L_{\max} = 16$, we observe empirically that the $0 \rightarrow 0$ constraints are computationally the most efficient. One important reason for that is that the positive matrices corresponding to $0 \rightarrow 0$ are

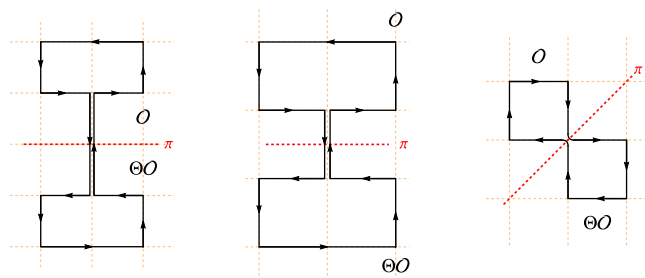


FIG. 5. Examples of three reflection symmetries on the lattice allowing new positivity conditions on WAs.

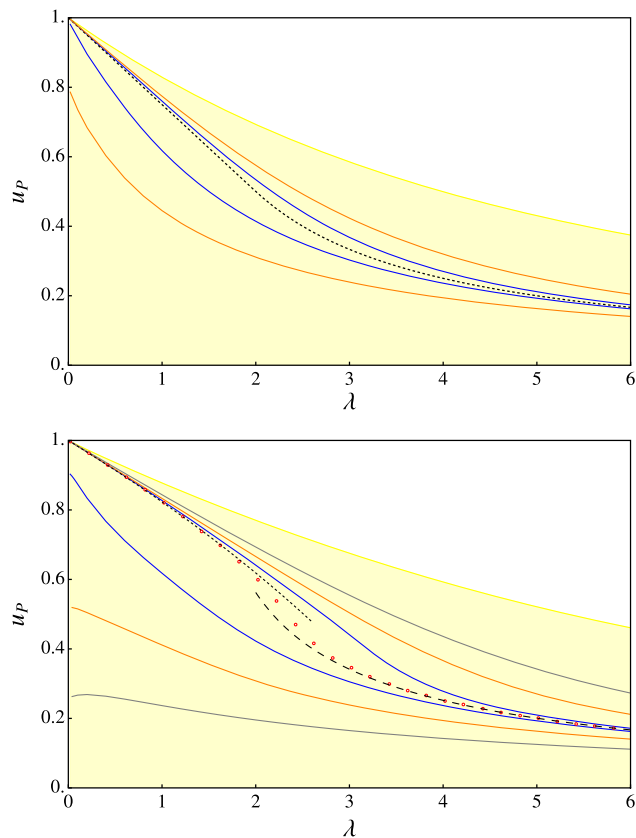


FIG. 6. u_p for 2D (upper) and 3D (lower) LGT: the upper and lower bounds from our bootstrap at $L_{\max} = 8$ (yellow region), $L_{\max} = 12$ (orange curves) and $L_{\max} = 16$ (blue curves). The 3D and $L_{\max} = 12$ result without reflection positivity (gray curve) is much less constraining. The line of red circles represents the MC data for $SU(10)$ LGT. The dashed black curve in the 2D plot is the exact solution (15). The dashed black curve in the 3D plot is the 3-loop PT result [37].

numerically more tractable with respect to symmetry reduction which we will discuss below.

B. Convex relaxation

In general, LEs are nonlinear. Here we use the relaxation method to replace all the nonlinear LE with linear ones where in the rhs we replace the products of WAs with new variables Q_{ij} , subject to extra constraints [17],

$$Q_{ij} = W_i W_j \xrightarrow{\text{replace}} \begin{pmatrix} 1 & W^T \\ W & Q \end{pmatrix} \geq 0. \quad (8)$$

Here $W = \{W_1, W_2, W_3, \dots\}$ denotes the column vector of all inequivalent WAs. Notice that the relaxation matrix has rank = 1 precisely when $Q_{ij} = W_i W_j$.

The LEs combined with the convex relaxation and positivity conditions constitute the constraints of semidefinite programming (SDP). To get rigorous bounds on WAs, we can maximize or minimize u_p .

C. Reduction by symmetry group

In conformal and S -matrix bootstraps, the positivity conditions are well-known to be organized in different spin channels [19,38] and different irreducible representations of global symmetry [39–42]. In parallel to that observation, we can greatly reduce the positivity matrices via the global lattice symmetries.

Formally, if we have an invariant group G preserving the inner product

$$\langle\langle g \circ \mathcal{O}_1 | (g \circ \mathcal{O}_2) \rangle\rangle = \langle \mathcal{O}_1 | \mathcal{O}_2 \rangle, \quad \forall g \in G \quad (9)$$

then the positivity condition on the matrix \mathcal{M} defined in Eq. (5) can be rearranged into a block-diagonal form corresponding to the irreps of G .

This well-studied procedure is known under the name “invariant semidefinite programming.” Here we refer to a statement [43] directly related to our current problem: *If the vector space of the paths can be decomposed as a direct sum of irreducible representations Rep_k of the invariant group with multiplicity m_k ,*

$$V = \bigoplus_{k=1}^D \text{Rep}_k^{\oplus m_k}, \quad (10)$$

then the positivity condition of the inner-product matrix is equivalent to the collection of positivity conditions on the matrices corresponding to each Rep_k , with matrix dimension $m_k \times m_k$.

For the correlation matrix $0 \rightarrow 0$, the invariant group G is $B_d \times \mathbb{Z}_2$, where B_d is the hyperoctahedral group in d spacetime dimensions. It acts on a Wilson path by corresponding rotations and reflections on the spacetime lattice. \mathbb{Z}_2 is the group action reversing the path.

For the reflection-positivity matrices $0 \rightarrow 0$ the invariant groups are subgroups of $B_d \times \mathbb{Z}_2$, leaving the reflection plane invariant. These invariant subgroups are summarized in Table I.

Implementing this symmetry reduction is similar to projecting the physical state with respect to spin and parity in conformal or S -matrix bootstrap. Practically, we do the following steps:

- (1) Find a specific realization of every irrep of the invariant group using GAP software [44].

TABLE I. Invariant groups of correlation and reflection matrices.

Dimension	Hermitian conjugation	Site and link reflection	Diagonal reflection
2	$B_2 \times \mathbb{Z}_2$	$\mathbb{Z}_2 \times \mathbb{Z}_2$	$\mathbb{Z}_2 \times \mathbb{Z}_2$
3	$B_3 \times \mathbb{Z}_2$	$B_2 \times \mathbb{Z}_2$	\mathbb{Z}_2^3
4	$B_4 \times \mathbb{Z}_2$	$B_3 \times \mathbb{Z}_2$	$B_2 \times \mathbb{Z}_2^2$

- (2) Use the algorithm initiated in [45] to find an equivalent real representation (if the irrep by GAP is complex).
- (3) To decompose into such irreps, we use the projector to Rep_k [46],

$$p_{\alpha\alpha,k} = \frac{\dim(\text{Rep}_k)}{\dim G} \sum_{g \in G} r_{\alpha\alpha}(g^{-1})g. \quad (11)$$

Here $r_{\alpha\beta}$ is a matrix element of a real representation identified at step 2, and $\alpha, \beta = 1, 2, \dots, \dim(\text{Rep}_k)$. Taking $\alpha = 1$, $P_k = p_{11,k}$ gives us a projector to Rep_k .

D. Selection of multiplets of Wilson paths

The Wilson paths form different multiplets of the invariant group. Within each multiplet, the symmetry group permutes different Wilson paths. When constructing the positivity matrices, some multiplets are more important than others. We kept only the most important multiplets. More precisely, several WAs are not related to other WAs by the LEs, such as the 4×4 square Wilson loop at $L_{\max} = 16$. We believe that such WAs and the open Wilson paths out of which they are constructed are relatively unimportant.

As an example, take the correlation matrix for the paths $0 \rightarrow 0$ at $3D$ and $L_{\max} = 16$. It has a huge size 6505×6505 . After the symmetry reduction and selection of the multiplets, the positivity of the correlation matrix reduces to positivity of 20 smaller matrices, each corresponding to its irrep, with sizes:

$$\begin{aligned} &38, 15, 25, 18, 62, 33, 68, 75, 56, 78, \\ &22, 18, 34, 15, 56, 33, 57, 76, 69, 73. \end{aligned} \quad (12)$$

So the SDP gets greatly simplified.

IV. DISCUSSION OF RESULTS

Here we present the results of computation of plaquette average $u_P(\lambda)$ for various bare couplings λ in LGT in $2D$, $3D$, and $4D$. On Fig 1 we compare our bootstrap data in $4D$ with MC for $SU(10)$ [15] and $SU(12)$ [25] LGT, assuming that, with our accuracy, $N_c = 10, 12$ are close enough to $N_c = \infty$. We also compare it with the known 3-loop $N_c = \infty$ PT result [47]:

$$u_P = 1 - \frac{\lambda}{8} - 0.005107\lambda^2 - 0.000794\lambda^3 + \mathcal{O}(\lambda^4) \quad (13)$$

as well as with the SC expansion valid in the SC phase, beyond the first-order phase transition point $\lambda_c \simeq 2.9$ [48],

$$u_P = \frac{1}{\lambda} + \frac{4}{\lambda^5} + \frac{60}{\lambda^9} + \frac{136}{\lambda^{11}} + \frac{1092}{\lambda^{13}} + \mathcal{O}(\lambda^{-15}). \quad (14)$$

The bootstrap bounds on u_P given for $L_{\max} = 8, 12, 16$ on Fig. 1 are quickly improving with the increase of cutoff. The physically most interesting WC phase is much better described by the upper bound. Moreover, we see that the upper bound nicely reproduces the 3-loop PT (13) for a large range of coupling, even beyond the phase transition point where PT is, strictly speaking, not valid. However, comparing these results to MC data, we see that it is not yet so good at capturing the departure from the PT in the interval (2.4, 2.8) where the MC data of [25] (given by black squares on Fig. 1) were used to compute the masses and the string tension. We expect a significant improvement for this range in our data if we reach $L_{\max} = 20$ or even 24. However, this will certainly demand much bigger computational resources.

Finally, we briefly discuss $2D$ and $3D$ cases. For $2D$ LGT the plaquette average can be computed exactly [49,50] (as well as any loop average, see [51]),

$$u_P = \begin{cases} 1 - \frac{\lambda}{4}, & \text{for } \lambda \leq 2 \\ \frac{1}{\lambda}, & \text{for } \lambda \geq 2. \end{cases} \quad (15)$$

This example was important for both checking our algorithm and for observing how fast our bootstrap data approach the exact result when increasing L_{\max} . The results are presented on Fig. 6. For physically interesting and challenging case of $3D$ LGT, we compare on Fig. 6 our bootstrap bounds at $L_{\max} = 8, 12, 16$ with the MC data [15] as well as with the known 3-loop PT [37] and SC [48] results. We observe a reasonably fast approach of bootstrap bounds to the MC data when increasing L_{\max} , but they are not as close to PT as in $4D$ case.

We employ in LEs the WAs up to the maximal length L_{\max} , so it can be considered as our infrared (IR) cutoff. The physical scale l_{ph} (set by inverse mass or square root of string tension) should, ideally, satisfy $1 \ll \frac{l_{ph}}{a_L} \ll L_{\max}$, where a_L is the lattice spacing. In this paper, we have, for the best of our data, $L_{\max} = 16$ which suggests that the window for the scale of measurable physical quantities in lattice units should be roughly $2 \lesssim \frac{l_{ph}}{a_L} \lesssim 6$ (compare it to Table 8 of [25] where the IR cutoff is set by the size of space-time torus, typically in the range 10to16, and the typical physical length is set by string tension $3 \lesssim \frac{l_{ph}}{a_L} \lesssim 6$).

We conclude that, even though the currently achieved values of L_{\max} in our bootstrap approach may be not sufficient to match the precision and scope of the MC experiments, especially for the confinement sensitive physics (glueball masses, string tension, etc.), our results give hope for a considerable improvement when augmenting

L_{\max} . Moreover, for sufficiently small couplings our upper bound data are already at least as good as MC.

V. PROSPECTS

The bootstrap procedure proposed here has a clear perspective for improving our results and advancing towards the computation of interesting observables. In particular, by choosing objective functions other than u_P , one can hope to get a better estimate for all involved physical quantities. For our current implementation at $L_{\max} = 16$, every data point takes ~ 20 hours of CPU time for $4D$, and only half an hour for $3D$ [52]. First, we want to increase the cutoff to $L_{\max} = 20$ and even to $L_{\max} = 24$. This will certainly need supercomputer power. From our current results, we expect a quick narrowing of our bounds to the accuracy comparable to, or even better than MC (without its toll of statistical and systematic errors). Furthermore, since in the 't Hooft limit we don't have internal fermion loops, we can try to find the quark condensate and hadron masses by simply summing up

the WAs with the spinorial factors for the relevant one- and two-point functions. The $1/N_c$ corrections (which might be small enough even for the physical $N_c = 3$ case) seem to be not insurmountable tasks since they are subject to linear LEs [9], with coefficients given by the solution of LE (3). One of such problems is the computation of glueball masses from the connected correlator of two small Wilson loops. One can also try to bootstrap directly the $N_c = 3$ YM theory, where the absence of large factorization could be compensated by multiple functional relations between WAs, absent for $N_c = \infty$ case.

ACKNOWLEDGMENTS

We thank Benjamin Basso, Maxim Chernodub, Alexander Gorsky, David Gross, Shota Komatsu, Marina Krstic-Marinkovic, Martin Kruczenski, Robert Pisarski, Jiaxin Qiao and Junchen Rong for useful discussions. V. K. thanks Kavli Institute for Theoretical Physics (KITP) of California University at Santa Barbara for kind hospitality during the work on this project.

-
- [1] G. S. Bali, C. Bauer, and A. Pineda, *Phys. Rev. D* **89**, 054505 (2014).
 - [2] M. Lüscher, *J. High Energy Phys.* 04 (2015) 142.
 - [3] M. Dalla Brida and M. Lüscher, *Eur. Phys. J. C* **77**, 308 (2017).
 - [4] L. Del Debbio, F. Di Renzo, and G. Filaci, *EPJ Web Conf.* **175**, 11023 (2018).
 - [5] M. G. Pérez, A. González-Arroyo, and M. Okawa, *J. High Energy Phys.* 10 (2017) 150.
 - [6] C. Gattringer and C. B. Lang, *Quantum Chromodynamics on the Lattice* (Springer, Berlin, 2010), Vol. 788.
 - [7] P. Weisz and P. Majumdar, *Scholarpedia* **7**, 8615 (2012).
 - [8] Y. M. Makeenko and A. A. Migdal, *Phys. Lett.* **88B**, 135 (1979); **89B**, 437(E) (1980).
 - [9] A. A. Migdal, *Phys. Rep.* **102**, 199 (1983).
 - [10] A. Jevicki, O. Karim, J. P. Rodrigues, and H. Levine, *Nucl. Phys.* **B213**, 169 (1983).
 - [11] A. Jevicki, O. Karim, J. P. Rodrigues, and H. Levine, *Nucl. Phys.* **B230**, 299 (1984).
 - [12] J. P. Rodrigues, *Nucl. Phys.* **B260**, 350 (1985).
 - [13] R. d. M. Koch, A. Jevicki, X. Liu, K. Mathaba, and J. a. P. Rodrigues, *J. High Energy Phys.* 01 (2022) 168.
 - [14] P. D. Anderson and M. Kruczenski, *Nucl. Phys.* **B921**, 702 (2017).
 - [15] P. Anderson and M. Kruczenski, *EPJ Web Conf.* **175**, 11011 (2018).
 - [16] H. W. Lin, *J. High Energy Phys.* 06 (2020) 090.
 - [17] V. Kazakov and Z. Zheng, *J. High Energy Phys.* 06 (2022) 030.
 - [18] R. G. Jha, *SciPost Phys. Lect. Notes* **46**, 1 (2022).
 - [19] R. Rattazzi, V. S. Rychkov, E. Tonni, and A. Vichi, *J. High Energy Phys.* 12 (2008) 031.
 - [20] D. Poland, S. Rychkov, and A. Vichi, *Rev. Mod. Phys.* **91**, 015002 (2019).
 - [21] M. F. Paulos, J. Penedones, J. Toledo, B. C. van Rees, and P. Vieira, *J. High Energy Phys.* 11 (2017) 133.
 - [22] A. L. Guerrieri, J. Penedones, and P. Vieira, *Phys. Rev. Lett.* **122**, 241604 (2019).
 - [23] J. Elias Miró and A. Guerrieri, *J. High Energy Phys.* 10 (2021) 126.
 - [24] See Supplemental Material at <http://link.aps.org/supplemental/10.1103/PhysRevD.107.L051501>, for more details.
 - [25] A. Athenodorou and M. Teper, *J. High Energy Phys.* 12 (2021) 082.
 - [26] A. Gonzalez-Arroyo and M. Okawa, *J. High Energy Phys.* 12 (2014) 106.
 - [27] M. Campostrini, A. Di Giacomo, and Y. Gunduc, *Phys. Lett. B* **225**, 393 (1989).
 - [28] M. Campostrini and A. Di Giacomo, *Phys. Lett. B* **197**, 403 (1987).
 - [29] G. S. Bali, C. Bauer, and A. Pineda, *Phys. Rev. Lett.* **113**, 092001 (2014).
 - [30] We thank Maxim Chernodub for discussion and suggestions on this subject.
 - [31] K. G. Wilson, *Phys. Rev. D* **10**, 2445 (1974).
 - [32] S. R. Wadia, *Phys. Rev. D* **24**, 970 (1981).
 - [33] Y. Makeenko, *Methods of Contemporary Gauge Theory*, Cambridge Monographs on Mathematical Physics (Cambridge University Press, Cambridge, England, 2005).

- [34] Jiaxin Qiao and Zechuan Zheng (to be published).
- [35] K. Osterwalder and E. Seiler, *Ann. Phys. (N.Y.)* **110**, 440 (1978).
- [36] I. Montvay and G. Münster, *Quantum Fields on a Lattice* (Cambridge University Press, Cambridge, England, 1997).
- [37] H. Panagopoulos, A. Skouroupathis, and A. Tsapalis, *Phys. Rev. D* **73**, 054511 (2006).
- [38] M. F. Paulos, J. Penedones, J. Toledo, B. C. van Rees, and P. Vieira, *J. High Energy Phys.* **12** (2019) 040.
- [39] R. Rattazzi, S. Rychkov, and A. Vichi, *J. Phys. A* **44**, 035402 (2011).
- [40] Y. He, A. Irrgang, and M. Kruczenski, *J. High Energy Phys.* **11** (2018) 093.
- [41] L. Córdova and P. Vieira, *J. High Energy Phys.* **12** (2018) 063.
- [42] M. F. Paulos and Z. Zheng, *J. High Energy Phys.* **05** (2020) 145.
- [43] C. Bachoc, D. C. Gijswijt, A. Schrijver, and F. Vallentin, in *Handbook on Semidefinite, Conic and Polynomial Optimization* (Springer, New York, 2012), pp. 219–269.
- [44] GAP, GAP—Groups, Algorithms, and Programming, Version 4.11.1 (The GAP Group, 2021).
- [45] N. Xu and P. Doerschuk, *SIAM J. Sci. Comput.* **43**, A3657 (2021).
- [46] J.-P. Serre, *Linear Representations of Finite Groups* (Springer, New York, 1977), Vol. 42.
- [47] B. Alles, A. Feo, and H. Panagopoulos, *Phys. Lett. B* **426**, 361 (1998); **553**, 337(E) (2003).
- [48] J.-M. Drouffe and J.-B. Zuber, *Phys. Rep.* **102**, 1 (1983).
- [49] D. J. Gross and E. Witten, *Phys. Rev. D* **21**, 446 (1980).
- [50] S. R. Wadia, [arXiv:1212.2906](https://arxiv.org/abs/1212.2906).
- [51] V. A. Kazakov and I. K. Kostov, *Phys. Lett.* **105B**, 453 (1981).
- [52] All the SDPs are solved by MOSEK [53].
- [53] M. ApS, MOSEK command line tools. Release 9.3.18 (2022), <https://docs.mosek.com/latest/cmdtools/index.html>.